Current Meter Performance in the Surf Zone*

STEVE ELGAR AND BRITT RAUBENHEIMER

Woods Hole Oceanographic Institution, Woods Hole, Massachusetts

R.T. GUZA

Scripps Institution of Oceanography, La Jolla, California

(Manuscript received 2 August 2000, in final form 12 April 2001)

ABSTRACT

Statistics of the nearshore velocity field in the wind–wave frequency band estimated from acoustic Doppler, acoustic travel time, and electromagnetic current meters are similar. Specifically, current meters deployed 25–100 cm above the seafloor in 75–275-cm water depth in conditions that ranged from small-amplitude unbroken waves to bores in the inner surf zone produced similar estimates of cross-shore velocity spectra, total horizontal and vertical velocity variance, mean currents, mean wave direction, directional spread, and cross-shore velocity skewness and asymmetry. Estimates of seafloor location made with the acoustic Doppler sensors and collocated sonar altimeters differed by less than 5 cm. Deviations from linear theory in the observed relationship between pressure and velocity fluctuations increased with increasing ratio of wave height to water depth. The observed covariance between horizontal and vertical orbital velocities also increased with increasing height to depth ratio, consistent with a vertical flux of cross-shore momentum associated with wave dissipation in the surf zone.

1. Introduction

Mean flows and wave-orbital velocities in the surf zone usually have been measured with electromagnetic current meters, but recently acoustic Doppler current meters also have been used. Although there are many comparisons of acoustic Doppler sensors with other current meters in the laboratory (Kraus et al. 1994; Voulgaris and Trowbridge 1998; and references therein) and in deep water (Andersen et al. 1999; Gilboy et al. 2000; and references therein), there are no detailed comparisons of electromagnetic and acoustic sensors in the surf zone. Here, acoustic Doppler, acoustic travel time, and electromagnetic current meters are compared for a range of nearshore wave conditions.

Previous studies in the surf zone have shown that the observed relationship between bottom pressure and horizontal velocity variance, integrated over the wind–wave frequency band, is consistent (errors less than 20%) with the theoretical transfer function of linear wave theory (Guza and Thornton 1980, and references therein). However, wavenumbers estimated with arrays of pressure gauges deployed in the nearshore and surf zone deviate from linear theory at frequencies between 2 and 3 times the power spectral peak frequency (Herbers et al. 2001, manuscript submitted to *J. Phys. Oceanogr.*, hereafter HESG). Here, deviations from linear theory of the complex transfer function between pressure and both horizontal and vertical velocities are examined as a function of frequency and of the ratio of wave height to water depth.

The instruments, field deployment, and data acquisition are described next (section 2), followed by comparisons of velocity statistics (section 3a), observations of nonlinearities (section 3b), and comparisons of estimates of seafloor elevation made with acoustic Doppler current meters and sonar altimeters (section 3c).

2. Observations

a. Field deployment and data acquisition

Current meters, sonar altimeters, and a pressure gauge were mounted on two frames deployed in the surf zone near the Scripps Institution of Oceanography pier, on the southern California coast. One frame (Fig. 1, top right) contained a Marsh–McBirney biaxial electromagnetic current meter (EMC1) with a 4-cm-diameter spherical probe (Aubrey and Trowbridge 1985; Guza et al. 1988), 3 SonTek acoustic Doppler OCEAN probes (5-MHz transmitter; Cabrera et al. 1987; Lohrmann et al.

*Woods Hole Oceanographic Institution Contribution Number 10241.

Corresponding author address: Steve Elgar, Applied Ocean Physics and Engineering, Woods Hole Oceanographic Institution, MS 11, Woods Hole, MA 02543.
E-mail: elgar@whoi.edu

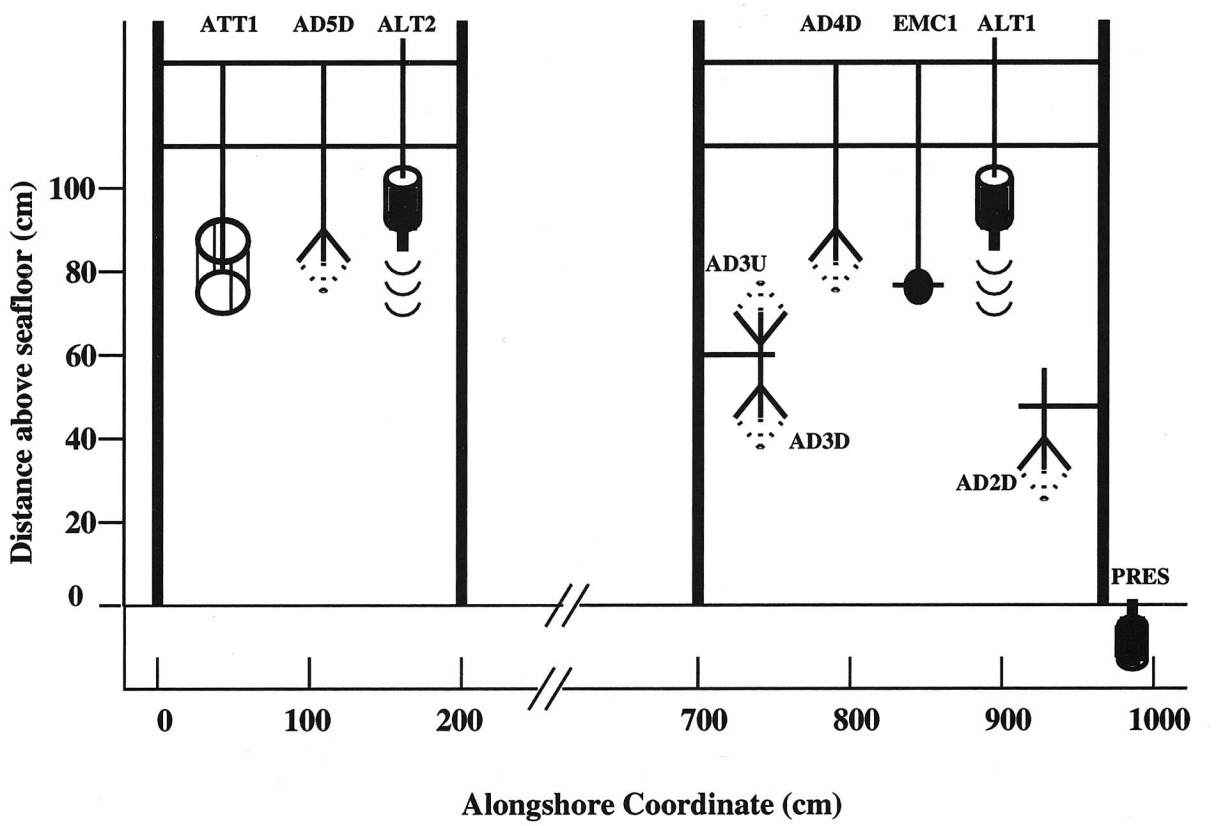

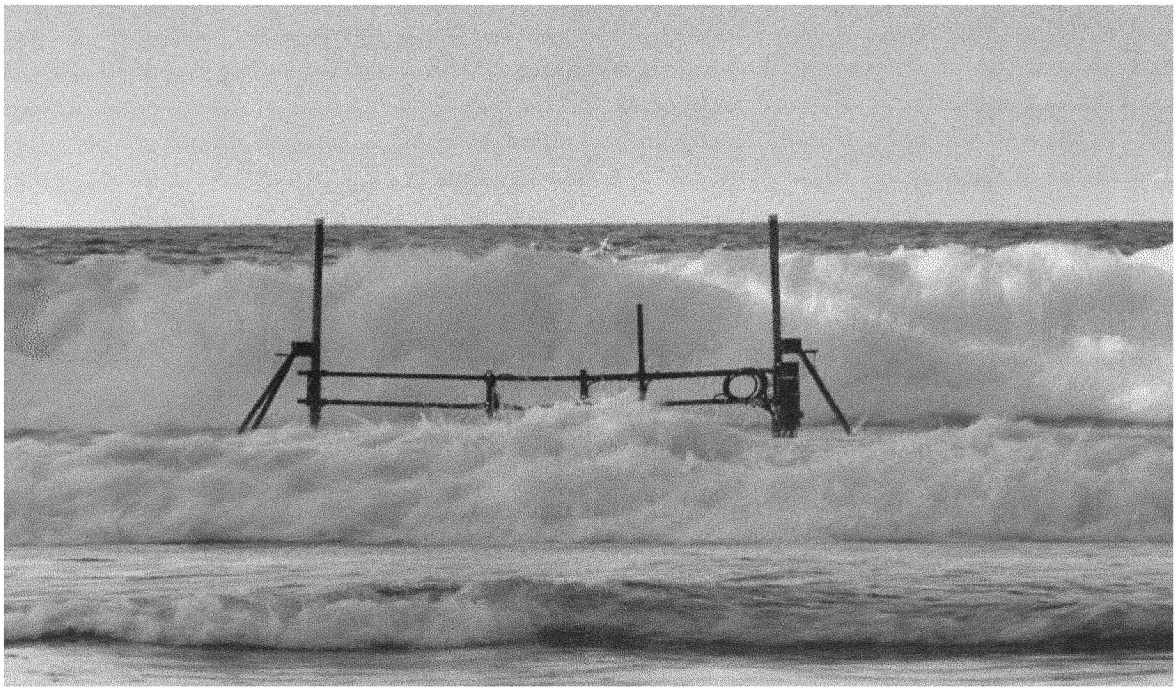

FIG. 1. (top) Schematic of frames and instruments that were deployed in the surf zone. The frames held one Marsh–McBirney electromagnetic current meter (EMC1), four SonTek OCEAN acoustic Doppler current meters mounted downward- (AD2D, AD3D, AD4D, AD5D) looking, and one mounted upward- (AD3U) looking, one MAVS acoustic travel time current meter (ATT1), two sonar altimeters (ALT1, ALT2), and a SETRA pressure gauge (PRES). (bottom) Photograph of the right-hand side frame (top) in the surf zone (courtesy of V. Polonichko).

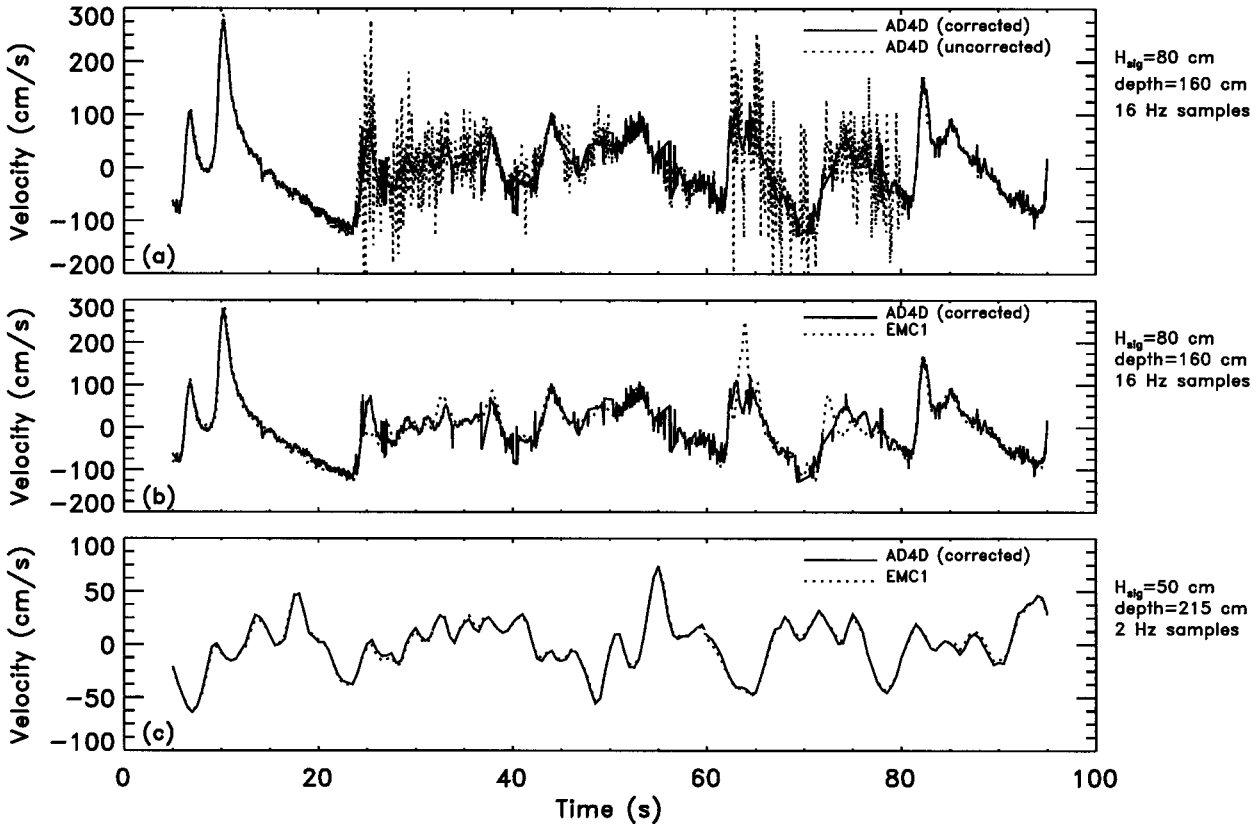

FIG. 2. Cross-shore velocity vs time. (a) Velocity reported by an acoustic Doppler velocimeter (AD4D) sampled at 16 Hz (dotted curve) and after correcting values with low correlations (solid curve). [H_{sig} = 80 cm, h = 160 cm.] (b) Corrected AD4D velocity time series [solid curve, same as (a)] and the velocity from a collocated electromagnetic current meter (EMC1) sampled at 16 Hz, but with a 2-Hz antialiasing filter (dotted curve). (c) Velocity time series (2-Hz sample rate) from AD4D (solid curve) and EMC1 (dotted curve) seaward of the surf zone. [H_{sig} = 50 cm, h = 215 cm.]

1994, 1995; Voulgaris and Trowbridge 1998), and a sonar altimeter (ALT1; Gallagher et al. 1996). Two of the acoustic Doppler sensors (AD2D and AD4D) were pointed down, and one was rotated from upward (AD3U) to downward (AD3D) looking during the deployment. A Setra pressure gauge (PRES) was deployed adjacent to a frame leg. A second frame (Fig. 1, top left) displaced about 5 m alongshore from the first frame contained a downward-looking SonTek acoustic Doppler OCEAN probe (AD5D), a sonar altimeter (ALT2), and a MAVS acoustic travel time current meter (ATT1; Williams et al. 1987). Cables connected the sensors to shore-based data acquisition computers and power supplies.

The sensing volumes of EMC1, AD4D, AD3U, ATT1, and AD5D were approximately 75 cm above the seafloor, and the sensing volumes of AD3D and AD2D were approximately 40 and 25 cm above the seafloor, respectively (Fig. 1). The sensors were aligned ($\pm 2°$) to the frames before deployment, and the frames were aligned ($\pm 5°$) with the shoreline by sighting along the cross bars with a handheld compass.

Data were acquired for 3072-s (51.2 min) periods every hour for 2 weeks during November 1999. All samples from both frames were controlled by a common shore-based clock. The instruments were deployed in water depths that ranged from 75 to 275 cm owing primarily to tidal fluctuations. Smaller depth changes caused by erosion and accretion occurred over several days (± 10 cm) and over tidal periods (± 1 cm). Significant wave heights (4 times the standard deviation of sea surface elevation fluctuations) ranged from 37 to 132 cm. The deployment location was in the surf zone most of the time (Fig. 1), and wave heights often were limited by breaking. The ratio γ of significant wave height (H_{sig}) to water depth (h) ranged from 0.21 to 0.64. The frequency f_p of the power spectral primary peak ranged from 0.055 to 0.160 Hz. Mean wave directions ranged from 0° to 15° relative to shore normal. Maximum 51.2-min mean cross-shore (U), alongshore (V), and vertical (W) currents were 20, 40, and 5 cm s^{-1}, respectively. Instantaneous horizontal velocities greater than 300 cm s^{-1} were observed.

b. Current meters and data reduction

The electromagnetic current meter measures the cross-shore and alongshore velocity in a volume within

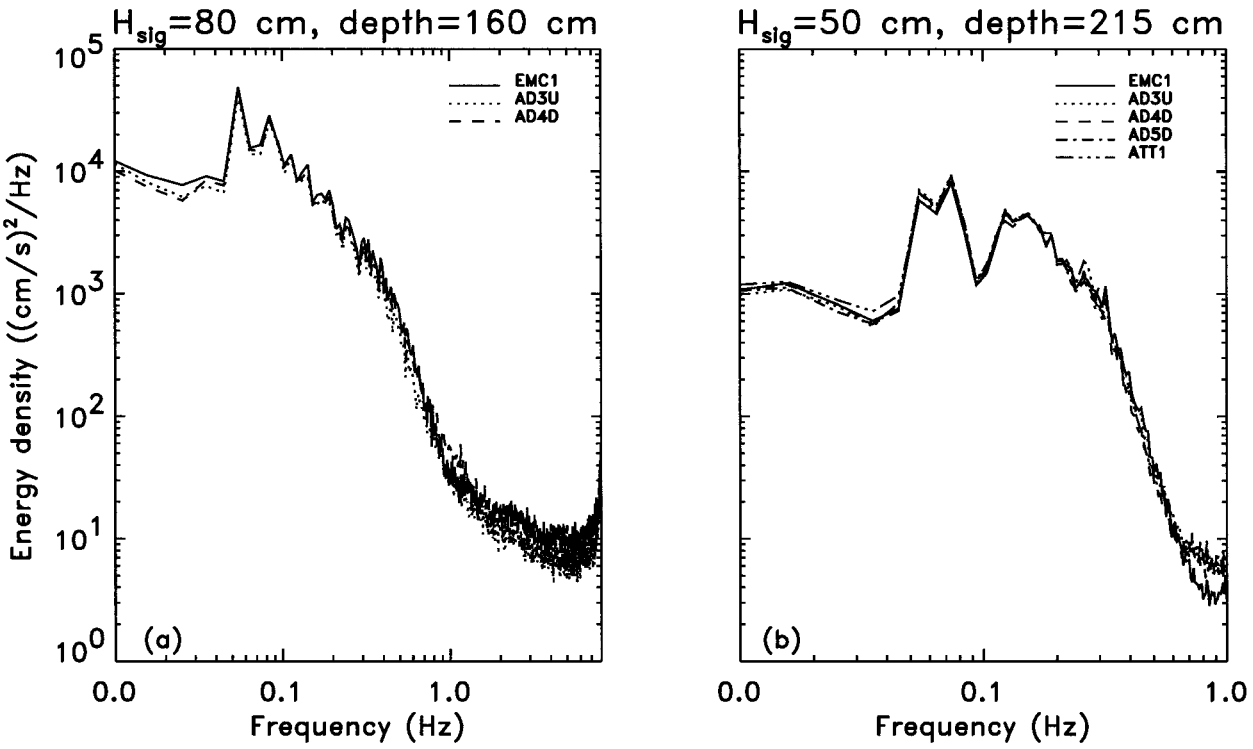

FIG. 3. Energy density of cross-shore velocity vs frequency for upward- (AD3U) and downward- (AD4D, AD5D) looking acoustic Doppler, acoustic travel time (ATT1), and electromagnetic (EMC1) current meters with sample volumes 75 cm above the seafloor. (a) Breaking waves in the surf zone, H_{sig} = 80 cm, h = 160 cm. The sample rate was 16 Hz. (EMC1 is not shown for frequencies above 1.5 Hz, where a 2-Hz antialiasing filter resulted in reduced energy density levels. ATT1 and AD5D were not operational.) (b) Nonbreaking waves seaward of the surf zone, H_{sig} = 50 cm, h = 215 cm. The sample rate was 2 Hz. (ATT1 is not shown for frequencies above 0.3 Hz, where occasional spikes from a malfunctioning circuit resulted in increased noise levels.) Spectra were estimated from six 512-s time series using a Hanning window with 75% overlap. Spectral estimates from five neighboring frequency bands were merged, yielding approximately 60 degrees of freedom and a frequency resolution of 0.01 Hz.

approximately 1 diameter (4 cm) of the spherical probe. Laboratory studies suggest the spherical electromagnetic sensors may be sensitive to free stream turbulence and wakes behind the probes (Aubrey and Trowbridge 1985). However, field studies have shown no evidence of large distortions owing to the complex flow field, although substantial errors in velocity measurements may occur when the sensor is near the free surface or seabed (Guza et al. 1988). Antialiasing filters in the electromagnetic current meter attenuated EMC1 signal levels above about 1.5 Hz.

The acoustic travel time current meter measures the average cross-shore, alongshore, and vertical velocity along the 10-cm-long acoustic path between two 12-cm diameter rings separated 7 cm in the vertical. Previous studies have shown these current meters to be accurate, even at low flow speeds (Williams et al. 1987). The acoustic travel time sensor (ATT1) had a maximum sample rate of 4 Hz.

Acoustic Doppler current meters transmit short acoustic pulses that are scattered back by reflectors in the water within the sample volume. For the parameters used here, the acoustic Doppler current meters measure the velocity within a cylindrical sample volume approximately 1.8-cm long and 1.2-cm diameter centered about 18 cm from the transducer. Using information about the instrument orientation and measurements along three beams, the average phase differences between several successive returns are converted into cross-shore, alongshore, and vertical velocities (Lhermitte and Serafin 1984; Cabrera et al. 1987; Brumley et al. 1991; Lhermitte and Lemmin 1994; Zedel et al. 1996; Voulgaris and Trowbridge 1998; and references therein). Bubbles and suspended sediment in the surf zone are strong reflectors, and the signal-to-noise ratio of the backscattered acoustic pulses usually is high. In contrast, the electromagnetic and acoustic travel time current meters do not require scatterers, and therefore would work equally well in clear water. The acoustic Doppler current meters, the altimeters, and the pressure gauge were sampled at rates ranging from 2 to 16 Hz.

Rapidly moving particles within the sample volume can result in successive returns from different scatterers, leading to inaccurate velocity estimates (Cabrera et al. 1987; Voulgaris and Trowbridge 1998). Furthermore, excessive scatterers (e.g., bubbles) near the sample volume can reflect sidelobe energy resulting in noisy velocity estimates. For example, 16-Hz velocity samples

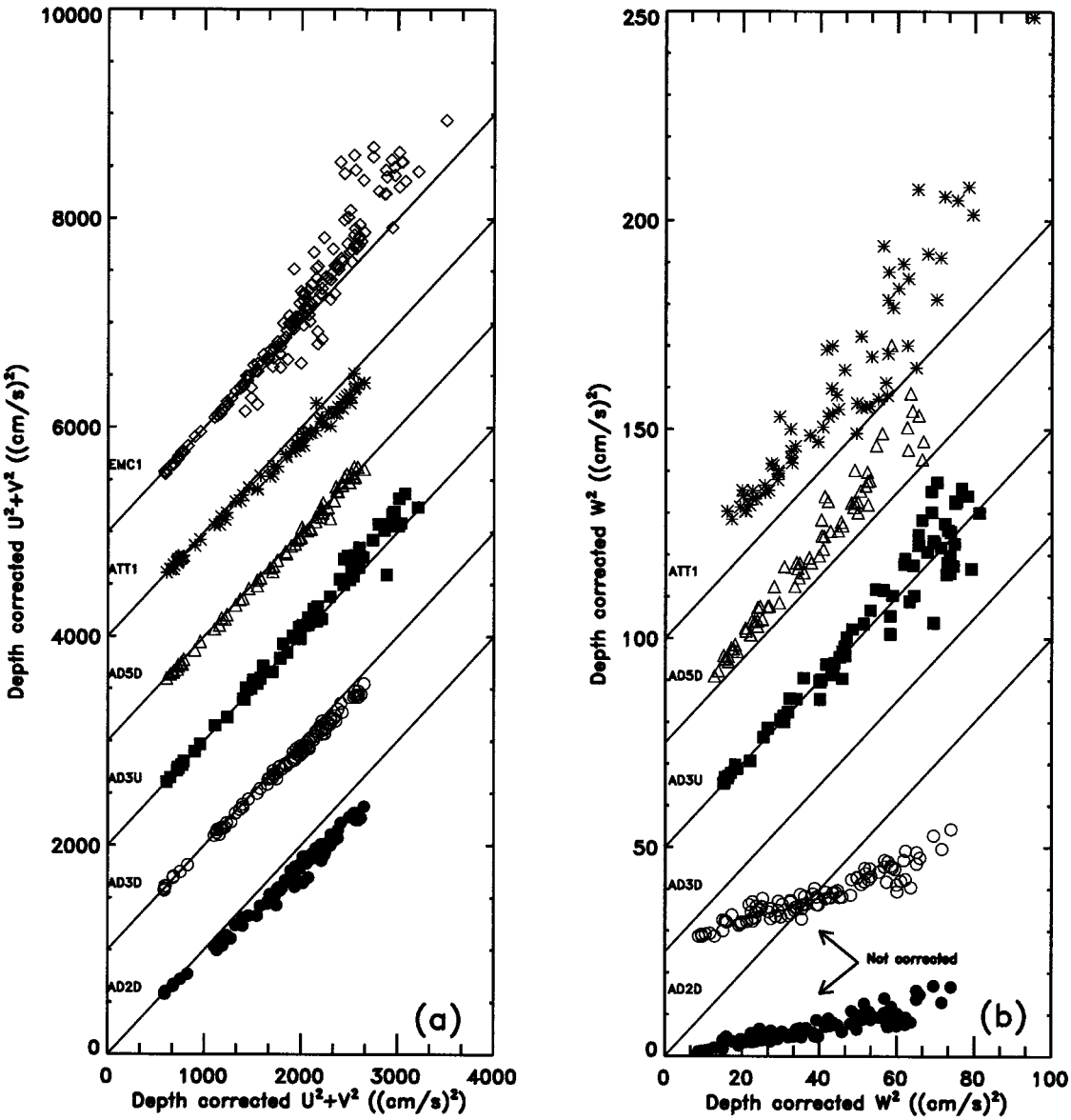

FIG. 4. Total (a) horizontal and (b) vertical velocity variance in the wind–wave frequency band ($0.05 < f < 0.30$ Hz) vs the variance estimated from time series acquired with downward-looking acoustic Doppler current meter AD4D (located 75 cm above the seafloor). The observed variances have been corrected to the equivalent variance 75 cm above the seafloor using linear theory [Eqs. (1)–(3)], except for the vertical variances [in (b)] of the two lowest acoustic Doppler sensors. Values of horizontal and vertical variances from successive sensors are vertically offset by 1000 and 25 $(\text{cm s}^{-1})^2$, respectively, for clarity.

in the surf zone ($H_{\text{sig}} = 80$ cm, $h = 160$ cm) are noisy (Fig. 2a, dotted curve), probably owing to bubbles from breaking waves, and the correlation (not shown) between successive returns is low.

The acoustic Doppler current meters report the correlation along the three beams, and thus postprocessing can identify potentially inaccurate measurements. The size of statistical fluctuations is approximately inversely proportional to the square root of the number of pulses per sample (i.e., proportional to the square root of the sample frequency s_f; Jenkins and Watts 1968). The correlation threshold used here was $0.3 + 0.4\ (s_f/25)^{1/2}$, which decreases as $(s_f)^{1/2}$ from the recommended (SonTek 1995) values of 0.7 for $s_f = 25$ Hz to 0.3 for mean currents (i.e., $s_f = 0$ Hz). Sequences of samples less than 1-s duration that fell below the threshold were replaced with values linearly interpolated between velocities before and after the incoherent sequence. Sequences of incoherent values longer than 1-s duration were replaced with a 1-s running mean of the values (Fig. 2a, solid curve). The amount of data with low correlations was not dependent on sample rates (not shown) nor on velocity values (e.g., for $0 <$ time < 20 s in Figs. 2a and 2b, the absolute value of the velocity

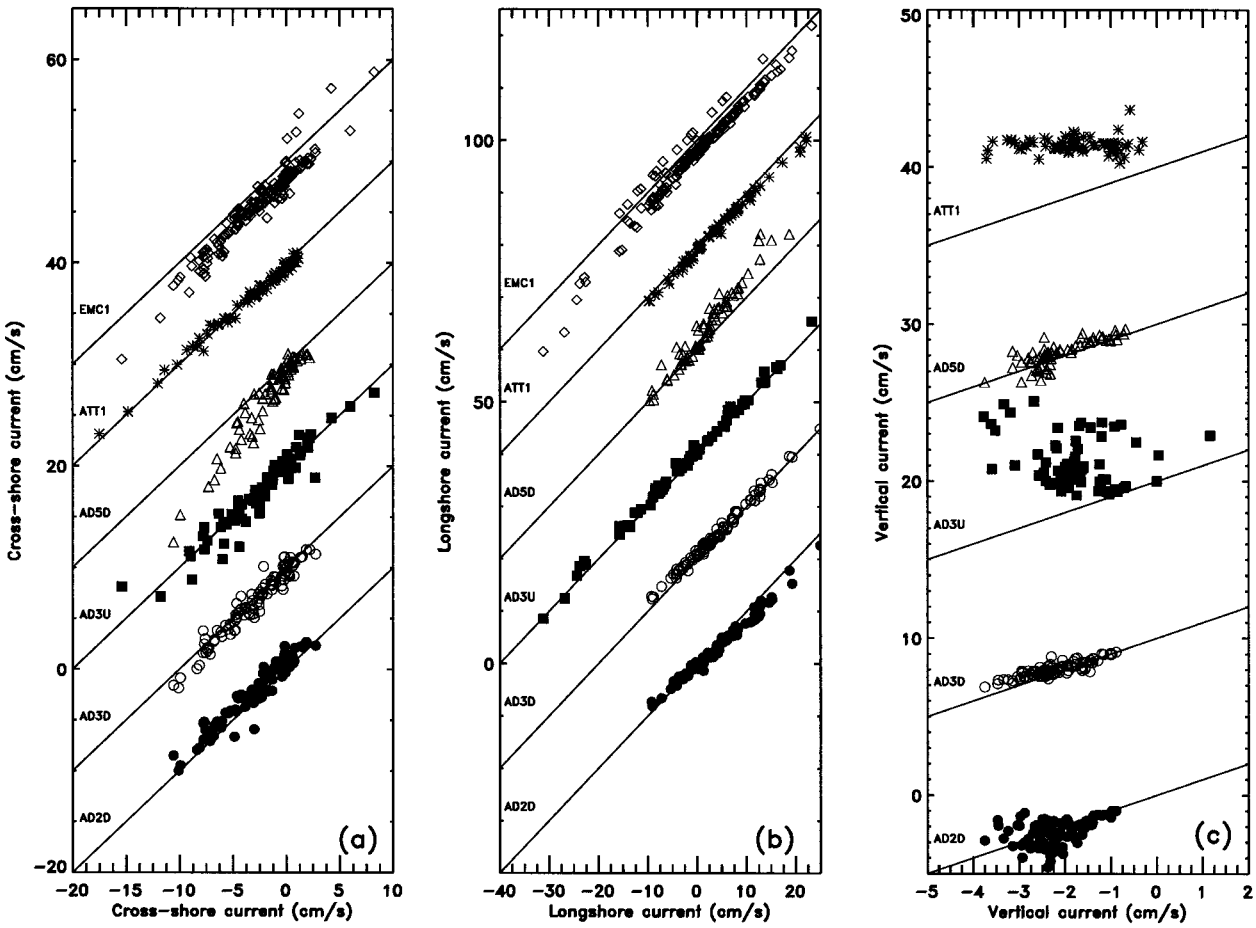

FIG. 5. (a) Cross-shore, (b) alongshore, and (c) vertical mean (51.2-min average) current vs the mean current obtained with downward-looking acoustic Doppler velocimeter AD4D (located 75 cm above the seafloor) except for the currents observed with ATT1, which are plotted vs AD5D (mounted on the same frame as ATT1). Negative cross-shore and vertical velocities are offshore- and downward-directed flows, respectively. Values of cross-shore, alongshore, and vertical mean currents from successive sensors are vertically offset by 10, 20, and 10 cm s^{-1}, respectively, for clarity.

varied from 0 to 300 cm s^{-1}, but there were no low correlation values, and AD4D is similar to EMC1). The percent of values with low correlations ranged from 0% for waves outside the surf zone (no bubbles) to about 2% for the downward-looking acoustic Doppler sensors for the largest breaking waves ($\gamma > 0.45$), which probably injected the most bubbles into the water column. The upward-looking acoustic Doppler (AD3U) could remain operational relatively closer to the surface than the downward-looking sensors because the transducer is submerged whenever the sensing volume (18 cm above the upward-looking transducer) is submerged, and as many as 8% of the values from AD3U were below the correlation threshold for the largest breaking waves.

Sensors sometimes were not submerged at low tide or in the wave troughs. The strength of the backscattered acoustic signal along each beam reported by the acoustic Doppler current meters was used to determine when sensors were out of the water. To avoid near-surface observations where the performance of all the current meters used here may be degraded, if more than 10 samples in a 51.2-min acoustic Doppler record had low signal-to-noise ratios, the time series from the acoustic Doppler, and from acoustic travel time and electromagnetic sensors at the same elevation, were discarded for that 51.2-min period.

The acoustic pulses emitted by the Doppler current meters also can be used to detect the presence of a boundary. After each 51.2-min data collection, the downward-looking acoustic Doppler current meters were used to estimate the distance to the seafloor every 3 s for 6.4 min.

3. Results

a. Current meter comparisons

Horizontal velocities (corrected for low correlations as described above) observed in the surf zone at 16 Hz with the acoustic Doppler current meters agree with

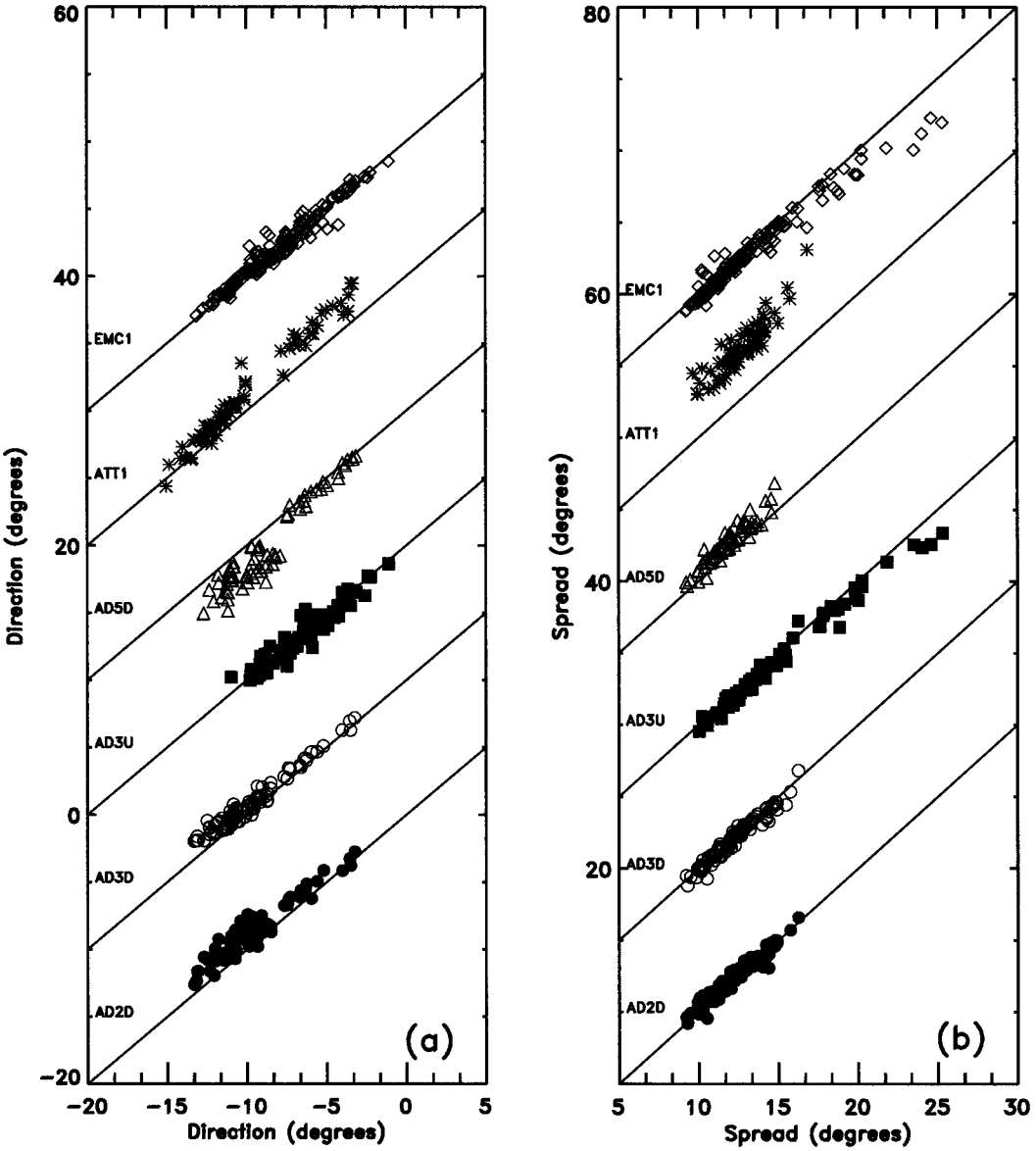

FIG. 6. (a) Mean direction and (b) directional spread of waves in the frequency band 0.05–0.30 Hz vs direction and spread estimated with observations from downward-looking acoustic Doppler current meter AD4D (located 75 cm above the seafloor), except for the directions and spreads estimated with ATT1, which are plotted vs AD5D (mounted on the same frame as ATT1). Values of direction and directional spread from successive sensors are vertically offset by 10° for clarity.

nearby electromagnetic current meter measurements, although some spikes remain in the acoustic Doppler time series (Fig. 2b, solid curve). When the sensors were seaward of the surf zone, differences between velocity time series obtained with acoustic Doppler and electromagnetic current meters are small (Fig. 2c, $H_{sig} = 50$ cm, $h = 215$ cm).

Energy density spectra of cross-shore velocity measured 75 cm above the seafloor with acoustic Doppler and electromagnetic current meters are similar both within the surf zone ($H_{sig} = 80$ cm, $h = 160$ cm, Fig. 3a) and seaward of the surf zone ($H_{sig} = 50$ cm, $h = 215$ cm, Fig. 3b). The horizontal velocity noise floor of the acoustic Doppler sensors within the surf zone was about 10 (cm s^{-1})^2/Hz, and was reached for frequencies above about 4 Hz, similar to the noise floor for the electromagnetic current meter (which had a 2-Hz antialiasing filter) at 1.5 Hz. The horizontal velocity noise floor seaward of the surf zone was lower, approximately 3 (EMC1) to 7 (AD3U, AD4D, AD5D) (cm s^{-1})^2/Hz, and was reached for frequencies above 1 Hz (not shown because the Nyquist frequency was 1 Hz for data shown in Fig. 3b). In both cases, noise levels for vertical velocities measured by the acoustic sensors were about

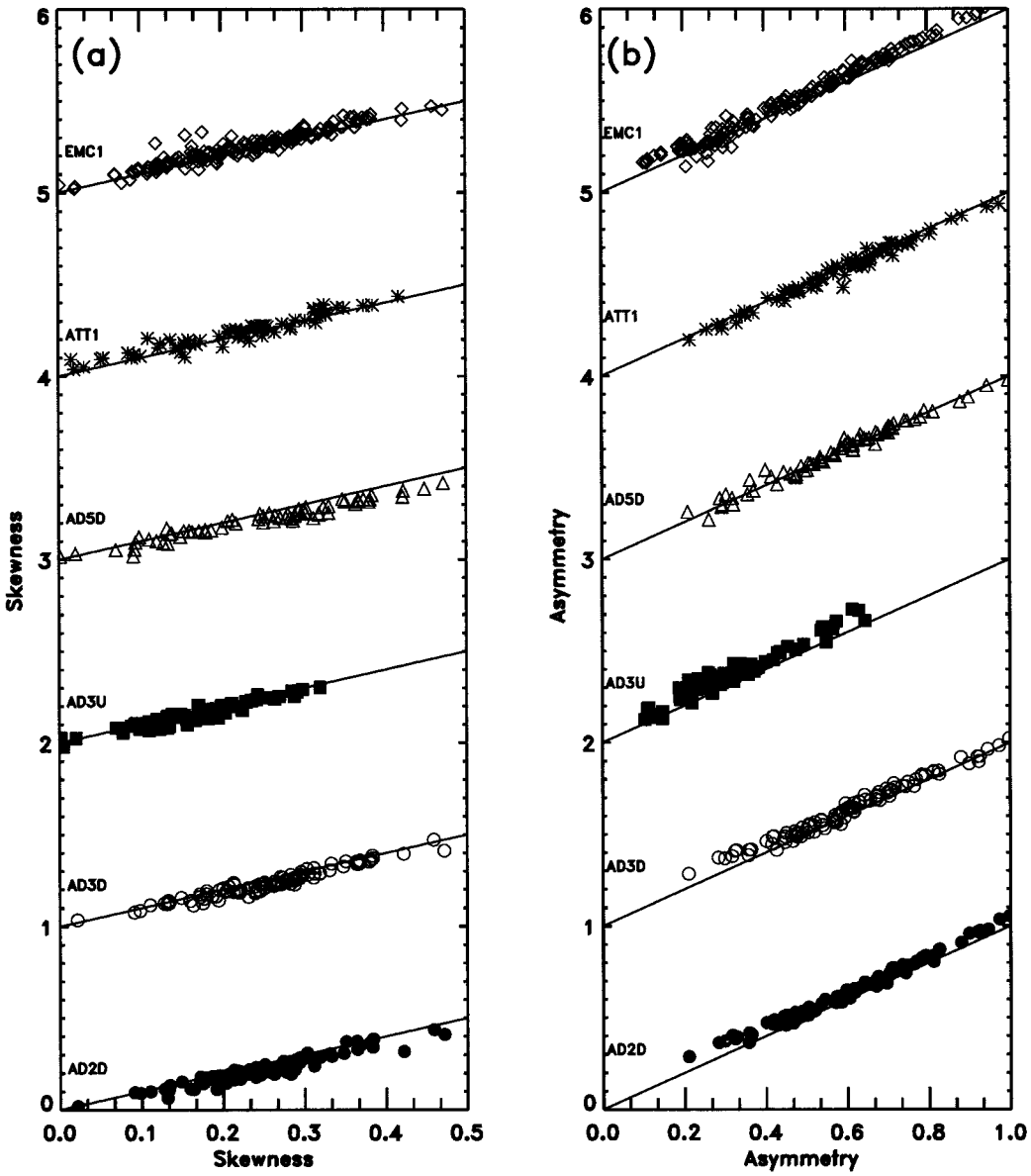

FIG. 7. Cross-shore velocity (a) skewness and (b) asymmetry in the frequency band 0.05–0.30 Hz vs skewness and asymmetry estimated from observations made with the downward-looking acoustic Doppler current meter AD4D (located 75 cm above the seafloor). Values of skewness and asymmetry from successive sensors are vertically offset by 1 for clarity.

one order of magnitude lower. The noise floors for the surf zone observations are consistent with theory (Cabrera et al. 1987; Brumley et al. 1991) and with laboratory results (Voulgaris and Trowbridge 1998). Occasional spikes in the ATT1 time series caused by a malfunctioning circuit resulted in high noise levels above about 0.3 Hz. For all conditions encountered the coherence between cross-shore velocity time series measured with neighboring sensors was close to 1.0 for frequencies below those affected by the noise floor (the spikes in ATT1 resulted in reduced coherences), and phase differences were less than a few degrees.

The total horizontal ($U^2 + V^2$) velocity variances in the wind–wave frequency band ($0.05 \leq f \leq 0.30$ Hz) determined from time series obtained with the different current meters usually differ by less than 10% (Fig. 4a). The relationship between horizontal velocity variances $U^2_{z_1}$ and $U^2_{z_2}$ for linear waves with radian frequency $\omega = 2\pi f$ at elevations z_1 and z_2 above the seafloor is (e.g., Mei 1983)

$$U^2_{z_2} = U^2_{z_1} \frac{\cosh^2(kz_2)}{\cosh^2(kz_1)}, \tag{1}$$

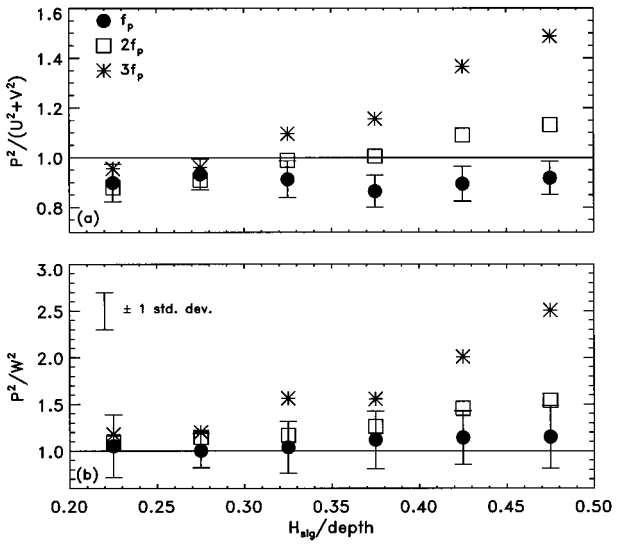

FIG. 8. Ratio of pressure variance to (a) horizontal and (b) vertical velocity variance {converted to pressure variance using linear theory [Eqs. (4) and (5), respectively]} vs ratio of significant wave height H_{sig} [based on pressure fluctuations in the band $0.05 < f < 0.30$ Hz and equation (6)] to water depth h. The 51.2-min records from AD4D, AD3U, and AD5D were sorted into 0.05-wide H_{sig}/h bins. Variance ratios are shown for the power spectral primary peak frequency (f_p) and its first two harmonics ($2f_p$, $3f_p$). Mean values for each bin and frequency are shown as symbols, with ±1 std dev bars shown for the values for f_p (std dev for the harmonics $2f_p$, $3f_p$ are similar). Linear theory [Eqs. (4) and (5)] predicts the ratios = 1.0. Note the different vertical scales in (a) and (b).

where the wavenumber k is given by the dispersion relationship

$$\omega^2 = gk \tanh kh, \tag{2}$$

and g is gravitational acceleration. Thus, linear theory predicts that wave-orbital horizontal velocities decrease only slightly over the vertical in these shallow depths, with a larger attenuation for high frequencies. The roughly 5% decrease in horizontal velocity variance between $z_2 = 75$ and $z_1 = 25$ cm above the seafloor is accounted for in Fig. 4 by using (1) and (2) to increase spectral levels to those 75 cm above the seafloor before integrating over the wind–wave frequency band. There is some scatter and a bias toward overestimates in the variances from the electromagnetic current meter for the strongest flows (Fig. 4a, cf. diamonds with the diagonal line), consistent with previous field studies (Guza et al. 1988). Variances estimated with upward- (AD3U) and downward- (AD4D) looking acoustic Doppler current meters are nearly equal at low flows (Fig. 4a, cf. filled squares with diagonal line), with slightly higher variances estimated with the upward-looking sensor for the most energetic flows. Relative to the downward-looking acoustic Doppler (AD4D) measurements 75 cm above the seafloor, the acoustic travel time current meter (ATT1) has a slight (less than 10%) bias toward underestimation of horizontal variance, as do the acoustic Doppler sensors (AD2D, AD3D) located closer to the seafloor. Horizontal velocity variance estimated with the two acoustic Doppler sensors (AD5D, AD4D) located 75 cm above the seafloor, but separated approximately 5 m alongshore are within a few percent for all conditions (Fig. 4a, cf. triangles with the diagonal line).

According to linear theory, at 75-cm elevation above the seafloor in 1.25-m water depth the horizontal velocity variance at $f = 0.10$ Hz is about 45 times the vertical velocity variance, and thus the measured vertical velocities may have small errors owing to sensor tilts of a few degrees. Although there is some scatter, vertical velocity variances measured 75 cm above the seafloor by upward- (AD3U) and downward- (AD4D, AD5D) looking acoustic Doppler current meters agree within about 20% (Fig. 4b, cf. filled squares and triangles with diagonal lines). The acoustic travel time current meter (ATT1) measured somewhat larger vertical velocity variance, perhaps owing to spikes in the time series. The relationship between vertical velocity variances $W^2_{z_1}$ and $W^2_{z_2}$ at elevations z_1 and z_2 above the seafloor is given by

$$W^2_{z_2} = W^2_{z_1} \frac{\sinh^2(kz_2)}{\sinh^2(kz_1)}. \tag{3}$$

Thus, vertical velocities (3) are attenuated more strongly over the water column than horizontal velocities (1), and 25 cm above the seafloor in 1.25-m depth the horizontal velocity variance at $f = 0.01$ Hz is almost 400 times the vertical velocity variance. Consequently, the measured vertical velocities at 25-cm elevation likely are corrupted by tilts of a few degrees in the vertical alignment of the sensors.

Mean horizontal currents measured with the different sensors are similar (Figs. 5a and 5b). Rip currents, which were visible from the neighboring pier, were observed occasionally to meander near the instrument frames, resulting in alongshore inhomogeneities in the mean flow field, and thus differences in mean horizontal currents observed at the two sensor frames, separated about 5 m alongshore (Figs. 5a and 5b, cf. triangles with diagonal lines). In contrast, mean cross- and alongshore currents measured with ATT1 and AD5D (located on the same instrument frame) are similar (Figs. 5a and 5b, cf. asterisks with diagonal lines). Mean vertical currents measured with the different sensors are less than about 4 cm s^{-1}. However, only the acoustic travel time current meter (ATT1), known to be accurate in low steady flows (Williams et al. 1987), measured approximately zero vertical flow (less than about 1 cm s^{-1}, which is not distinguishable from 0 for the instrument calibrations used here) for all conditions. Deviations from zero mean flows may be the result of flow blockage. The mean vertical flows measured by the downward-looking acoustic Doppler sensors (AD2D, AD3D, AD4D, and AD5D) differ from each other by less than 1 cm s^{-1} (cf. filled circles, open circles, and triangles with solid lines in Fig. 5c), whereas mean vertical flows measured

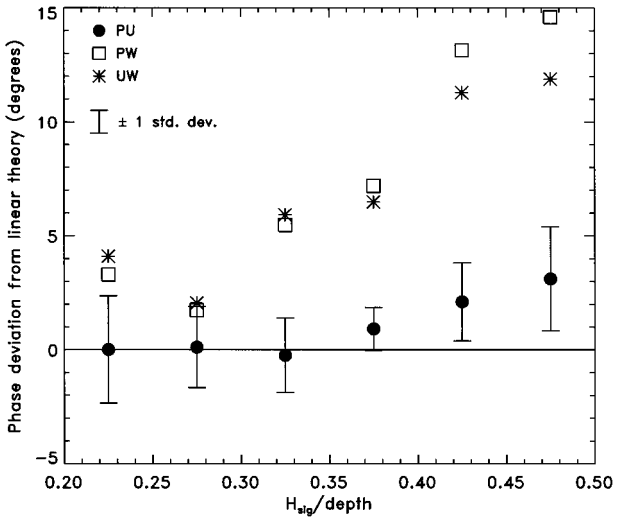

FIG. 9. Deviation from linear theory of the phase difference between pressure (P) and velocity fluctuations at f_p vs ratio of significant wave height H_{sig} ($0.05 < f < 0.30$ Hz) to water depth h. If linear theory is accurate, the phase deviation is 0. The 51.2-min records from AD4D were sorted into 0.05-wide H_{sig}/h bins. Mean values for each bin are shown as symbols, with ± 1 std dev bars shown for the deviations of the phase difference between pressure and cross-shore velocity (U, filled circles). Std dev for phase deviations between pressure and vertical velocity (W, open squares) and between cross-shore and vertical velocity (asterisks) are similar. At harmonic frequencies $2f_p$ and $3f_p$ phase deviations between P and U are similar to those at f_p, deviations between P and W are less than $\pm 3°$, and deviations between U and W are about half those at f_p.

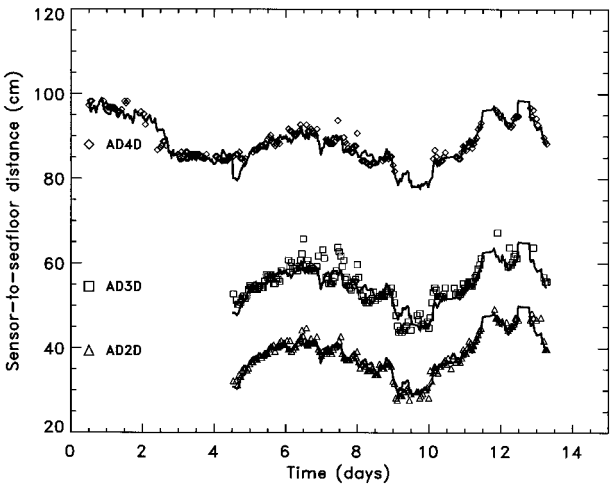

FIG. 10. Distance from the fixed sensor to the seafloor measured with acoustic Doppler current meters in boundary location mode (symbols) and with a sonar altimeter (ALT1, solid curves) mounted on the same frame. The acoustic current meter probes ranged from approximately 25–50 (AD2D), 45–65 (AD3D), to 80–100 (AD4D) cm above the slowly moving seafloor. (Velocity sample volumes are 18 cm below the probes.) The sonar altimeter was located approximately 75–95 cm above the seafloor, and estimates of its distance to the seafloor were converted to estimates that would have been obtained if the altimeter was collocated with each acoustic current meter. Agreement between measurements made with the acoustic Doppler current meter (AD5D) and the sonar altimeter (ALT2), both located approximately 75 cm above the seafloor on the other instrument frame, is comparable (not shown).

with the upward-looking AD3U are scattered relative to the downward-looking AD4D (cf. squares with solid line in Fig. 5c).

Mean wave direction (Fig. 6a) and directional spread (Fig. 6b) estimated from the covariance of U with V (Kuik et al. 1988) are similar for the time series acquired with the different current meters. The increased directional spread estimated by ATT1 is an artifact of the spikes caused by the malfunctioning circuit, leading to reduced covariance.

Third moments of wave-orbital velocities are important to sediment transport (Bowen 1980; Bailard 1981; and many others). Cross-shore velocity skewness (the mean of the cube of the demeaned cross-shore velocity time series normalized by the cross-shore velocity variance raised to the 3/2 power) and asymmetry [the mean of the cube of the Hilbert transform of the demeaned cross-shore velocity time series normalized by the cross-shore velocity variance raised to the 3/2 power (Elgar and Guza 1985)] estimated from time series acquired with the different current meters agree well [Fig. 7, average root-mean-square differences relative to AD4D are 0.03 (skewness) and 0.04 (asymmetry)]. The spikes in time series acquired with ATT1 occur in pairs, one positive and one negative, and thus cancel in odd moments (e.g., mean, skewness, and asymmetry).

b. Nonlinearities

Linear wave theory often is used to convert between bottom pressure, sea surface elevation, and wave-orbital velocity. For example, the ratios of the variance of pressure ($P^2_{z_p}$) at a location z_p above the bottom to the variance of horizontal ($U^2_{z_u} + V^2_{z_u}$) and vertical ($W^2_{z_u}$) velocities at a location z_u above the bottom are, respectively,

$$\frac{P^2_{z_p}}{U^2_{z_u} + V^2_{z_u}} = \frac{\omega^2}{(gk)^2} \frac{\cosh^2(kz_p)}{\cosh^2(kz_u)} \tag{4}$$

$$\frac{P^2_{z_p}}{W^2_{z_u}} = \frac{\omega^2}{(gk)^2} \frac{\cosh^2(kz_p)}{\sinh^2(kz_u)}. \tag{5}$$

Similarly, the ratio of sea surface elevation variance (η^2) to pressure variance is

$$\frac{\eta^2}{P^2_{z_p}} = \frac{\cosh^2(zh)}{\cosh^2(kz_p)}. \tag{6}$$

Nearshore and surf zone significant wave heights, estimated by applying linear theory transfer functions to bottom pressure or near-bottom wave-orbital velocity spectra and integrating the resulting sea surface elevation spectra over the wind–wave frequency band, differ by less than 10% from the wave heights obtained with surface-piercing wave staffs (Guza and Thornton 1980;

and references therein). However, the effects of nearly resonant triad nonlinear interactions can become strong in shallow water, especially at frequencies corresponding to harmonics of the power spectral primary peak (f_p). For the conditions here, the relationship between the spectral density of wave-orbital horizontal velocities and bottom pressure fluctuations at f_p is within 10% of linear theory for the full range of observed wave height to water depth ratios γ (Fig. 8a). However, when γ is larger than about 0.35, linear theory tends to underpredict the observed transfer function between horizontal velocity and pressure fluctuations at harmonic frequencies ($2f_p$, $3f_p$), with the deviations increasing as γ increases. Similarly, the observed relationship between vertical velocity and pressure fluctuations at the spectral primary peak frequency is consistent with linear theory, but motions at harmonic frequencies increasingly deviate from linear theory with increasing γ (Fig. 8b). The deviations from linear theory observed here may be associated with 20%–30% deviations from linear theory of wavenumbers at harmonic frequencies, similar to those observed with arrays of pressure gauges in the surf zone (HESG).

Phases between pressure, cross-shore velocity, and vertical velocity fluctuations are consistent (within about 4°) with linear theory for γ less than about 0.3, but deviate increasingly with increasing γ (Fig. 9). Deviations from 90° of the phase between U and W correspond to nonzero covariance of U with W ($\langle UW \rangle$). Above the bottom boundary layer nonzero $\langle UW \rangle$ can occur if the seafloor slopes (Chu and Mei 1970), if there is a cross-shore gradient in wave amplitude owing to breaking-induced dissipation or bottom friction (Mei 1983; Deigaard and Fredsoe 1989), or if there are depth-varying mean currents (Peregrine 1976). The vertical variation of $\langle UW \rangle$ in these cases is discussed by Rivero and Arcilla (1995), but has not been measured in the surf zone. Consistent with nonzero $\langle UW \rangle$ owing to dissipation-induced cross-shore gradients in wave amplitude, the deviations of the observed U–W phase (asterisks in Fig. 9) from the quadrature predicted by linear theory for a flat bottom, as well as values of $\langle UW \rangle$ (not shown), increase with increasing γ, with $\langle UW \rangle$ about 3% of $\langle UU \rangle$ for the highest values of γ. The value of $\langle UW \rangle$ is close to zero when wave breaking is minimal ($\gamma \approx 0.2$, not shown), implying bottom slope effects are negligible 75 cm above the seafloor, consistent with Chu and Mei (1970). The $\langle UW \rangle$ are positive in the coordinate system used here (e.g., positive U is onshore directed, and positive W is upward flow). Further study is needed to determine if flow blockage distorted the measured vertical flows.

c. Seafloor location

The acoustic Doppler current meters can operate in a mode where the distance to the nearest strongly reflecting boundary, in this case the seafloor, is measured. The distance to the seafloor estimated with acoustic Doppler current meters located 25–100 cm above the bed deviated by less than 5 cm from estimates made with a sonar altimeter designed to operate in the surf zone (Gallagher et al. 1996; Fig. 10).

4. Summary

Statistics of the nearshore and surf zone velocity field in the wind–wave frequency band estimated with acoustic Doppler, acoustic travel time, and electromagnetic current meters deployed 25–100 cm above the seafloor are similar. In particular, the different current meters produced similar estimates of cross-shore velocity spectra, total horizontal and vertical velocity variance, mean currents, mean wave direction, directional spread, and cross-shore velocity skewness and asymmetry. Signal-to-noise ratios of acoustic returns can be used to determine when the acoustic Doppler sensors are out of the water, and alongbeam correlations between successive returns can be used to detect inaccurate velocity estimates. Inaccurate samples were replaced either by interpolation or by a 1-s running mean (if the noisy samples spanned more than 1 s), producing more accurate velocities. Estimates of seafloor location made with collocated acoustic Doppler sensors and sonar altimeters differed by less than a few cm. Deviations from linear theory in the relationship between pressure and both horizontal and vertical velocity fluctuations were observed to increase with increasing ratio of wave height to water depth, and with increasing frequency. The observed covariance between horizontal and vertical orbital velocities also increased with increasing height-to-depth ratio, consistent with a vertical flux of cross-shore momentum associated with wave dissipation in the surf zone.

Acknowledgments. Engineering and field support were provided by William Boyd, Dennis Darnell, Kimball Millikan, Kelly Rankin, William Schmidt, and Brian Woodward during inconveniently energetic surf zone conditions (Fig. 1 was not the most extreme case). Financial support was provided by the Office of Naval Research.

REFERENCES

Anderson, S., E. Terray, J. R. White, and A. Williams III, Eds.,1999: *Proceedings of the IEEE Sixth Working Conference on Current Measurement.* IEEE Cat. No. 99CH36331, 322 pp.

Aubrey, D., and J. Trowbridge, 1985: Kinematic and dynamic estimates from electromagnetic current meter data. *J. Geophys. Res.*, **90,** 9137–9146.

Bailard, J., 1981: An energetics total load sediment transport model for a plane sloping beach. *J. Geophys. Res.*, **86,** 10 938–10 954.

Bowen, A. J., 1980: Simple models of nearshore sedimentation: Beach profiles and longshore bars. *The Coastline of Canada,* S. B. McCann, Ed., Geological Survey of Canada Paper 80-10, 1–11.

Brumley, B., R. Cabrera, K. Deines, and E. Terray, 1991: Performance

of a broad-band acoustic Doppler current profiler. *IEEE Oceanic Eng.*, **16,** 402–503.

Cabrera, R., K. Deines, B. Brumley, and E. Terray, 1987: Development of a practical coherent acoustic Doppler current profiler. *Proc. Oceans '87*, Halifax, NS, Canada, IEEE Oceanic Engineering Society, 93–97.

Chu, V., and C. Mei, 1970: On slowly varying Stokes waves. *J. Fluid Mech.,* **41,** 873–887.

Diegaard, R., and J. Fredsoe, 1989: Shear stress distribution in dissipative water waves. *Coastal Eng.,* **13,** 357–378.

Elgar, S., and R. Guza, 1985: Observations of bispectra of shoaling surface gravity waves. *J. Fluid Mech.,* **161,** 425–448.

Gallagher, E., B. Boyd, S. Elgar, R. Guza, and B. Woodward, 1996: Performance of a sonar altimeter in the nearshore. *Mar. Geol.,* **133,** 241–248.

Gilboy, T., T. Dickey, D. Sigurdson, X. Yu, and D. Manov, 2000: An intercomparison of current measurements using a vector measuring current meter, an acoustic Doppler current profiler, and a recently developed acoustic current meter. *J. Atmos. Oceanic Technol.,* **17,** 561–574.

Guza, R., and E. Thornton, 1980: Local and shoaled comparisons of sea surface elevations, pressures, and velocities. *J. Geophys. Res.,* **85,** 1524–1530.

——, M. Clifton, and F. Rezvani, 1988: Field intercomparisons of electromagnetic current meters. *J. Geophys. Res.,* **93,** 9302–9314.

Herbers, T., S. Elgar, N. Sarap, and R. Guza, 2001: Dispersion properties of surface gravity waves in shallow water. *J. Phys. Oceanogr.*, submitted.

Jenkins, G., and D. Watts, 1968: *Spectral Analysis and Its Applications.* Holden-Day, 525 pp.

Kraus, N., A. Lohrmann, and R. Cabrera, 1994: New acoustic meter for measuring 3D laboratory flows. *J. Hydraul. Eng.,* **120,** 406–412.

Kuik, A., G. van Vledder, and L. Holthuijsen, 1988: A method for routine analysis of pitch-and-roll buoy data. *J. Phys. Oceanogr.,* **18,** 1020–1034.

Lhermitte, R., and R. Serafin, 1984: Pulse-to-pulse coherent Doppler signal processing techniques. *J. Atmos. Oceanic Technol.,* **1,** 293–308.

——, and U. Lemmin, 1994: Open-channel flow and turbulence measurement by high-resolution Doppler sonar. *J. Atmos. Oceanic Technol.,* **11,** 1295–1308.

Lohrmann, A., R. Cabrera, and N. Kraus, 1994: Acoustic-Doppler velocimeter (ADV) for laboratory use. *Proc. Conf. on Fundamentals and Advancements in Hydraulic Measurements and Experimentation*, Buffalo, NY, American Society of Civil Engineers, 351–365.

——, G. Gelfenbaum, and J. Haines, 1995: Direct measurement of Reynold's stress with an acoustic Doppler velocimeter. *Proc. IEEE Fifth Conf. on Current Measurements*, St. Petersburg, FL, IEEE Oceanic Engineering Society, 205–210.

Mei, C., 1983: *The Applied Dynamics of Ocean Surface Waves.* Wiley Interscience, 728 pp.

Pergerine, D., 1976: Interaction of water waves and currents. *Adv. Appl. Mech.,* **16,** 9–117.

Rivero, F., and A. Arcilla, 1995: On the vertical distribution of $\langle \tilde{u}\tilde{w} \rangle$. *Coastal Eng.,* **25,** 137–152.

SonTek, 1995: ADV operation manual, version 1.0. [Available from SonTek, 6837 Nancy Ridge Drive, Suite A, San Diego, CA 92121.]

Voulgaris, G., and J. Trowbridge, 1998: Evaluation of the acoustic Doppler velocimeter (ADV) for turbulence measurements. *J. Atmos. Oceanic Technol.,* **15,** 272–289.

Williams, A., J. Tochko, R. Koehler, T. Gross, W. Grand, and C. Dunn, 1987: Measurement of turbulence with an acoustic current meter array in the oceanic bottom boundary layer. *J. Atmos. Oceanic Technol.,* **4,** 312–327.

Zedel, L., E. Hay, and A. Lohrmann, 1996: Performance of single beam pulse-to-pulse coherent Doppler profiler. *IEEE J. Oceanic Eng.,* **21,** 290–299.